Comparison Study of Constitutive Models for Overconsolidated Clays

Z. Wan[a] , Y. P. Yao[b,] , Z.W. Gao[c]

(a. Research Institute of Base and Foundation, China Academy of Building Research, Beijing 100013, China;
b. School of Transportation Science and Engineering, Beihang University, Beijing 100091, China;
c. School of Engineering, University of Glasgow, Glasgow, G12 8QQ, UK)

SUMMARY

Widely distributed in natural deposits, the overconsolidated (OC) clays have attracted extensive experimental investigations on their mechanical behaviors, especially in the 1960s and 1970s. Based on these results, numerous constitutive models have also been established. These models generally fall into two categories: one based on the classical plasticity theory and the other the bounding surface (BS) plasticity theory, with the latter being more popular and successful. The BS concept and the subloading surface (SS) concept are the two major BS plasticity theories. The features of these two concepts and the representative models based on them are introduced respectively. The unified hardening (UH) model for OC clays is also based on the BS plasticity theory but distinguishes itself from other models by the integration of the reference yield surface, unified hardening parameter, potential failure stress ratio and transformed stress tensor. Modification is made to the Hvorslev envelop employed in the UH model to improve its capability of describing the behaviors of clays with extremely high overconsolidation ratio (OCR) in this paper. The comparison among the BS model, SS model and UH model is performed. Evidence shows that all these three models can characterize the fundamental behaviors of OC clays, such as the stress dilatancy, strain softening and attainment of the

critical state. The UH model with the revised Hvorslev envelop has the fewest parameters which are identical to those of the modified Cam-Clay model.

KEY WORDS: Clay, Overconsolidation, Critical state, Bounding surface, Subloading surface, Unified hardening model

1. Introduction

Most naturally deposited clays involve some degree of overconsolidation due to processes of loading and unloading such as tamping, cyclic loading, erosion, excavations, and changes in ground-water tables. OC clays behave distinctively from the normally consolidated (NC) clays, like strain softening and shear dilatancy. The research on constitutive models for OC clays has always been a hot topic and the achievements are abundant. These models generally fall into two categories: one based on the classical plasticity theory and the other the BS theory, with the latter being more successful and popular. The models of the first category will be briefly reviewed and three representative models of the second type will be introduced in detail and compared in this paper.

The original and modified Cam-Clay models are the most fundamental models for clays, which are developed based on the classical incremental plasticity theory and the critical state soil mechanics [1-3]. The two models can describe behaviors of the NC and lightly OC clays but fail to capture those of the highly OC clays quite satisfactorily. Nevertheless, they, together with the critical state soil mechanics [4-5], laid a solid foundation for future research on the constitutive models for OC clays.

Some other researchers have also developed models for OC clays based on the classical

plasticity theory and the critical state soil mechanics. Pender [6] proposed an elastoplastic model to characterize behaviors of OC clays on the basis of the conventional triaxial compression test results and the critical state soil mechanics by introducing some assumptions for different stress paths. This model has only four parameters and can describe the fundamental behaviors of OC clays. However, it is concerned only with the behaviors of clays under an applied stress system such that the intermediate and minor principal stresses are equal and thus the influence of the intermediate principal stress on the behaviors of OC clays is not taken into account. Through studying the response of clays subjected to undrained shear conditions, Banerjee et al. [7, 8] derived both associated and non-associated stress-strain relations using the incremental plasticity theory. A unified state parameter model for clay and sand was developed by Yu [9] based on the critical state soil mechanics. The behavior of OC clays can also be modeled by it. But the classical plasticity theory has its own restriction that no plastic strain can occur inside the yield surface and it always gives an abrupt transition from being elastic to being elastoplastic for the stress-strain relations of OC clays.

Mroz proposed a workhardening model for metals by introducing the concept of a field of hardening moduli featured by a series of nested configuration surfaces associated with a large number of state variables [10]. This concept can overcome the restriction of the classical plasticity theory mentioned above to some extent. Following the work by Mroz, Prévost developed a model to describe behaviors of clays subjected to different stress paths, such as monotonic and cyclic undrained loading [11]. The performance of such models are generally better than those based on the classical plasticity theory, but more

configuration surfaces are required in order to get better accuracy. Complexity arises from the memory of a large number of configuration surfaces and the corresponding state variables. However, this concept inspired the development of the BS plasticity theory. The distinctive feature of the BS theory is that plastic deformation can occur inside a "reference" yield surface.

Despite the different names given, the BS concept [12-13] and subloading surface (SS) concept [14-16] are the two major BS plasticity theories. Explicit definition of the loading surface is unnecessary when using the BS concept, while for the SS concept, a normal yield surface is defined explicitly and the subloading surface is assumed to be geometrically similar to it. The BS model was originally developed for metals subjected to cyclic loading and later applied to the constitutive modeling for OC clays by Dafalias et al. [17-20]. Other researchers have also used the BS concept to model the behaviors of OC clays. A general model for OC clays was developed by Mroz et al. by incorporating the BS concept [21-22]. The MIT-E3 constitutive model for OC clays proposed by Whittle et al. was also based on the BS concept [23]. Within the framework of the BS plasticity theory, Rouainia and Wood developed a kinematic hardening structure model by integrating the reference surface, the bubble surface, and the structural surface [24]. This model is able to characterize the behaviors of both structural and OC clays. Hashiguchi et al. developed the SS concept to describe the behaviors of materials with elastic-plastic transition and also applied it to the constitutive modeling for both sand and OC clays [25-26]. Subsequently, some further applications of the SS concept in the constitutive models for clays appeared. Nakai et al. developed the subloading t_{ij} model for OC clays by

integrating the t_{ij} model for NC clays and the SS concept [27-28]. By introducing the superloading surface to describe the structural evolution of clays, Asaoka proposed the superloading surface model for structural clays which can also describe the behaviors of OC clays [29-31]. For OC clays, the superloading surface model is the same as the SS model.

Recently, Yao et al. proposed the UH model for OC clays by integrating the current yield surface, reference yield surface, potential failure stress ratio and unified hardening parameter as well as employing the transformed stress tensor based on the spatial mobilized plane (SMP) criterion [32]. The BS concept and SS concept opened up new avenues for the development of constitutive models for OC clays, and various models have been established based on them. The unified hardening parameter, potential failure stress ratio and transformed stress tensor make the UH model distinct from other models for OC clays, although it is also based on the BS plasticity theory. In the following sections, two models for OC clays as representatives for those based on the BS and SS concepts respectively and the UH model will be introduced. Modification is made to the Hvorslev envelop employed in the UH model to improve its capability of describing the peak strength characteristics of highly OC clays. Capabilities of these models in describing the behaviors of OC clays will be analyzed by comparing the model predictions with the test results on the Fujinomori clay subjected to constant mean stress triaxial compressions. The predicted undrained effective stress paths of the models in the *q*-*p* plane and the corresponding projections in the *e*-*p* plane will be illustrated to investigate the model capabilities in describing the critical state characteristics of OC clays.

2. Bounding Surface Model

The BS model for OC clays developed by Dafalias and Herrmann [19] is a representative for those based on the BS concept. This model is in the premise of the critical state soil mechanics, and the critical state characteristics for OC clays can be readily described.

In this model, the stress variables p, q , S and Lode's angle α are employed:

$$p=\frac{\sigma_{kk}}{3};\quad q=\left(\frac{3}{2}s_{ij}s_{ij}\right)^{1/2};S=\left(\frac{1}{3}s_{ij}s_{jk}s_{ki}\right)^{1/3};-\frac{\pi}{6}\le\alpha=\frac{1}{3}\sin^{-1}\left[\frac{27}{2}\left(\frac{S}{q}\right)^{3}\right]\le\frac{\pi}{6}\ (1)$$

where σ_{ij} is the Cauchy stress tensor, $s_{ij}=\sigma_{ij}-p\delta_{ij}$, p is the mean stress and q is the general deviatoric stress.

As the employment of the yield surface of the modified Cam-Clay model over-predicts the peak strength of highly OC clays, a BS consisting of two ellipses and one hyperbola is proposed to overcome this shortcoming. The hardening rule is the same as that for the modified Cam-Clay model, which is expressed as

$$\frac{dp_0}{de^p}=-\frac{\langle p_0-p_l\rangle+p_l}{\lambda-\kappa};\quad de^p=-(1+e_0)\,d\varepsilon_v^p \tag{2}$$

where p_0 is the intersection of the BS and the p-axis, e^p is interpreted as the plastic void ratio related to the plastic volumetric strain ε_v^p, p_l is a model constant to ensure that the elastic bulk modulus will not become zero when the mean stress is zero, λ and κ are the compression index and swelling index, respectively, and e_0 is the initial void ratio.

The radial mapping rule is adopted in the BS model and can be expressed as

$$\bar{p}=b(p-p_c)+p_c;\bar{q}=bq;\bar{S}=bS;\bar{\alpha}=\alpha \tag{3}$$

where p_c represents the location of the mapping center on the p-axis, the stress invariants

with an upper bar are associated with the BS, b is an intermediate variable characterizing the distance between the current stress point and the "image" stress point, which can be solved by substituting the radial mapping rule equations into the functions of the BS on condition that the current stresses and p_0 are known. The mapping rule plays an important role in the BS model as it affects both the dilatancy and hardening. The associated flow rule is adopted on the BS, and the plastic flow direction is determined at the "image" stress point.

The bounding plastic modulus $\overline{K}_p$ corresponding to the "image" stress state can be obtained based on the condition of consistency

$$\overline{K}_p = \frac{3(1+e_0)}{(\lambda-\kappa)}\left(\left\langle 1-\frac{p_l}{p_0}\right\rangle+\frac{p_l}{p_0}\right)\frac{\partial F}{\partial \overline{p}}\left(\frac{\partial F}{\partial \overline{p}}+\frac{\partial F}{\partial \overline{q}}\right) \tag{4}$$

The plastic modulus K_p of the current stress state is defined as a function of $\overline{K}_p$ and the shape hardening function $\hat{H}$

$$K_p = \overline{K}_p + \hat{H}\left\langle \frac{b}{b-1}-s\right\rangle^{-1} \tag{5}$$

$$\hat{H} = \frac{1+e_0}{\lambda-\kappa} g^{*2} p_a\left[z^m h(\alpha)+(1-z^m)h_0\right] \tag{6}$$

where

$$g^{*2} = \left(\frac{\partial F}{\partial \overline{p}}\right)^2+\left(\frac{\partial F}{\partial \overline{q}}\right)^2 \tag{7}$$

$$z = \frac{qR}{3\sqrt{3}Np_0} \tag{8}$$

$$h(\alpha) = \frac{2(h_e/h_c)}{1+h_e/h_c-(1-h_e/h_c)\sin 3\alpha}h_c \tag{9}$$

$$N = \frac{2(N_e/N_c)}{1+N_e/N_c-(1-N_e/N_c)\sin 3\alpha}N_c \tag{10}$$

$$R = \frac{2(R_e/R_c)}{1+R_e/R_c-(1-R_e/R_c)\sin 3\alpha} R_c \tag{11}$$

$$h_0 = (h_e + h_c)/2 \tag{12}$$

in which F is the function of the BS, p_a is the atmospheric pressure, m, s, h_e, h_c, N_e and N_c are the model parameters, $\langle\ \rangle$ is the Macauley bracket, and δ_{ij} is the Kronecker delta. Equations (9)-(12) are actually interpolation functions for the parameters, which can make the BS model reproduce more realistic behaviors of OC clays in the three-dimensional stress space. When the clay is overconsolidated, the current stress state lies inside the BS, b>1 and $K_p > \overline{K}_p$. As the plastic deformation proceeds, the distance between the current stress state and the "image" stress state becomes smaller and smaller and finally approaches zero at the critical state. The OCR is gradually lost during this process. When the clay is normally consolidated or at the critical state, the current stress state lies on the BS, b=1 and $K_p = \overline{K}_p$.

3. Subloading Surface Model

The SS concept was originally developed for the materials exhibiting a gradual transition from the elastic to fully plastic state, like metals. The salient feature of the SS concept is that the current stress state always lies on the SS, which retains a geometrical similarity to the normal yield surface. The plastic modulus at the current stress state is described by the ratio of the size of the SS to that of the normal yield surface. For OC clays, this ratio also reflects the OCR, and the behavior of NC clays can be described when it is equal to unity. The SS model is also based on the critical state soil mechanics. The associated flow rule is adopted to both the subloading surface and normal yield surface, and the plastic flow

direction is determined at the current stress state.

The model proposed by Hashiguchi and Collins [26] will be introduced here. For the isotropic OC clays under monotonic loading conditions, it can be assumed that $\alpha_{ij} = \beta_{ij} = s_{ij} = \bar{\alpha}_{ij} = 0$ [26]. So the formulation of the subloading surface can be written as

$$f = p\left(1+\chi^2\right) = RF\left(H\right) \tag{13}$$

$$p = \mathrm{tr}\left(\sigma_{ij}\right),\ \ \sigma^*_{ij} = \sigma_{ij} - p\delta_{ij},\ \ \eta_{ij} = \sigma^*_{ij}/p,\ \ \chi = \left\|\eta_{ij}\right\|/m \tag{14}$$

$$m = \frac{2\sqrt{6}\sin\varphi}{3-\sin\varphi\sin 3\theta},\ \ \sin 3\theta = -\sqrt{6}\frac{\mathrm{tr}\left(\eta_{im}\eta_{mn}\eta_{nj}\right)}{\left\|\eta_{ij}\right\|^3} \tag{15}$$

where α_{ij} and $\bar{\alpha}_{ij}$ are reference points, s_{ij} is the similarity center, β_{ij} is the rotational hardening variable, φ is the friction angle, R is the similarity-ratio, H is the hardening variable for the normal yield surface, and $F\left(H\right)$ represents the size of the normal yield surface, which is the same as that of the modified Cam-Clay model here.

The evolution law of the similarity-ratio is given by

$$dR = U\left\|D^p_{ij}\right\| \ \text{ for } \ \left\|D^p_{ij}\right\| \geq 0 \tag{16}$$

$$U = -u\ln R \tag{17}$$

where D_{ij} is the plastic stretching, $\|\ \|$ stands for the magnitude, and u is a material constant. It can be seen that R decreases due to plastic deformation and reaches unity at the critical state.

The elastic bulk modulus K and shear modulus G change with not only the mean stress but also the magnitude of the hardening function F in the SS model introduced here. Such definitions are more reasonable from the perspective of thermodynamics and can overcome some of the intrinsic irrationality of those employed in the BS and UH models [26]. However, the intention of this paper is to analyze how the SS model describes the

behavior of OC clays and thus its plastic property is of more significance. So the classical definitions based on the *e*-ln*p* linear relation will be adopted to the SS model

$$K = \frac{p(1+e_0)}{\kappa} \tag{18}$$

$$G = \frac{3(1-2\nu)}{2(1+\nu)}K \tag{19}$$

where ν is the Poisson's ratio. This can also facilitate the comparison among the models.

4. Unified Hardening Model

Both the BS model and SS model are capable of modeling the characteristic behaviors of OC clays, but some parameters without clear physical significances are introduced. An appropriate constitutive model for soil should be able to capture the characteristic behaviors of soil, but its accuracy is of less importance [6]. An ideal situation is that all the parameters have clear physical significances and can be determined from the conventional laboratory tests directly. The UH model for OC clays with the revised Hvorslev envelop has the same parameters as the modified Cam-Clay model and can capture the characteristic behaviors of OC clays. The main features of this model will be elaborated in the following section.

The UH model is similar to the SS model. The current stress state lies on the current yield surface, the hardening parameter of which is the unified hardening parameter *H*, and the reference stress point lies on the reference yield surface, which is identical to that of the modified Cam-Clay model. The similarity center of these two surfaces is the origin of the *p*-*q* space. The ratio of the size of the current yield surface to that of the reference yield surface reflects the OCR. When the clay is normally consolidated or at the critical state,

the current yield surface coincides with the reference yield surface. The Hvorslev envelope, which is widely used to determine the peak strength of OC clays, is adopted in this model. The transformed stress tensor based on the SMP criterion is employed in the model to describe the behavior of overconsolidated clays in the three-dimensional stress space.

The reference yield surface is the same as that of the modified Cam-Clay model

$$\bar{f} = \ln\frac{\bar{p}}{\bar{p}_0} + \ln\left[1+\frac{\bar{q}^2}{M^2\bar{p}^2}\right] - \frac{1}{c_p}\int d\varepsilon_v^p = 0 \tag{20}$$

where $\bar{p}$ is the mean principal stress of the reference stress point, $\bar{q}$ is the deviator stress corresponding to the reference stress point, $\bar{p}_0$ is the initial intersect of the reference yield surface and the p-axis, $c_p = (\lambda-\kappa)/(1+e_0)$, and M is the stress ratio at the critical state in triaxial compression.

The current yield surface and the unified hardening parameter can be written as

$$f = \ln\frac{p}{p_0} + \ln\left[1+\frac{q^2}{M^2p^2}\right] - \frac{1}{c_p}\int dH = 0 \tag{21}$$

$$H = \int dH = \int \frac{M_f^4-\eta^4}{M^4-\eta^4}\,d\varepsilon_v^p = \int \frac{1}{\Omega}\,d\varepsilon_v^p \tag{22}$$

$$M_f = \left(\frac{1}{R}-1\right)(M-M_h)+M \tag{23}$$

$$R = \frac{p}{\bar{p}} = \frac{q}{\bar{q}} = \frac{p}{\bar{p}_0}\left(1+\frac{\eta^2}{M^2}\right)\exp\left(-\frac{\varepsilon_v^p}{c_p}\right) \tag{24}$$

where p_0 is the initial mean principal stress, M_h is the slope of the Hvorslev envelope in the $p-q$ plane, M_f is defined as the potential failure stress ratio, and R is the OC parameter which increases as the OCR decreases. For OC clays, the potential stress ratio M_f is larger than the critical state stress ratio at the initial stage. It decreases as the

plastic deformation proceeds and finally becomes equal to the critical state stress ratio at the critical state. The associated flow rule is adopted to the current yield surface and the plastic flow direction is determined at the current stress state.

The hardening parameter *H* controls the hardening and softening of the current yield surface and has the following features:

In the hardening region, dH is always non-negative. The following conclusions can be drawn from Equation (22):

(1) Under isotropic compression condition, $\eta = 0$, we have $d\varepsilon_v^p = dH$ for NC clay and $d\varepsilon_v^p = \left(M^4 / M_f^4\right) dH$ for OC clay with $M^4 / M_f^4 < 1$, which reflects the fact that the compressibility of OC clay under isotropic compression state is smaller than that of the corresponding NC clay.

(2) When $0 < \eta < M$, $d\varepsilon_v^p > 0$, which describes positive dilatancy.

(3) When $\eta = M$, $d\varepsilon_v^p = 0$, which corresponds to the point of characteristic state. Note that at this state, as $M^4 - \eta^4 = 0$, $M_f^4 - \eta^4 > 0$ and $d\varepsilon_v^p = 0$, thus $dH = \dfrac{M_f^4 - \eta^4}{M^4 - \eta^4} d\varepsilon_v^p > 0$. So the current yield surface still expands.

(4) When $M < \eta < M_f$, $d\varepsilon_v^p < 0$, which means negative dilatancy and strain hardening.

With the stress ratio η increasing and the potential stress ratio M_f decreasing continuously, η will catch up with M_f and finally exceeds it at a certain time. After that, the strain softening process commences. In the softening region, since $\eta > M_f > M$, $d\varepsilon_v^p < 0$, $dH < 0$. At the critical state, $\eta = M = M_f$ and $d\varepsilon_v^p = dH = 0$.

As can be seen, the potential stress ratio M_f related to the OC parameter *R* and the

slope of the Hvorslev envelope controls both the hardening of the current yield surface and the predicted peak strength of OC clays. So it plays a cardinal role in the UH model. However, the Hvorslev envelope overestimates the strength of OC clays with high OCRs, as it gives non-zero strength even when the mean effective stress is zero. So the UH model over-predicts the peak strength of highly OC clays. It is reasonable to incorporate both the zero-tension line and the Hvorslev envelope to describe the peak strength of highly OC clays. But it is not convenient to employ them in the constitutive modeling as they are not continuous. Actually, Dafalias and Herrmann [19] have used a BS consisting of two ellipses and one hyperbola with continuous tangents at the connecting points in stead of a single one to control the predicted peak strength of highly OC clays. But the predicted peak stress ratio may still be larger than 3, which means the clay can sustain tensile stress. An appropriate strength locus for OC clays should approach the zero-tension line as the OCR increases to infinite and lies between the critical state line (CSL) and yield surface passing point C in the *q*-*p* space as shown in Figure 1. A parabola-shaped Hvorslev envelop satisfying such requirements can be proposed

$$\left(q_f - q_0\right)^2 = 2\beta\left(p - p_0\right) \tag{25}$$

where point (p_0, q_0) is the vertex of the parabola, β is a parameter for the parabola controlling the curvature, and point (p, q_f) lies on the parabola.

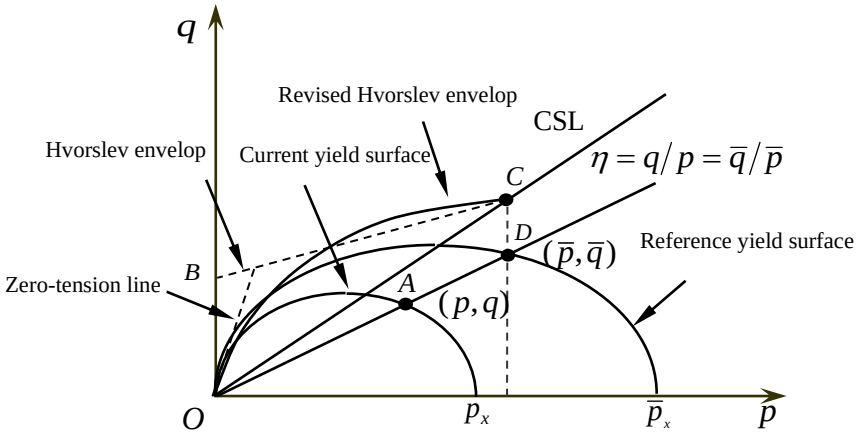

Fig. 1. Current yield surface, reference yield surface and the Hvorslev envelop

When *R*=1, the revised Hvorslev envelope intersects with the CSL at point C $(\bar{p}, M\bar{p})$. So

$$\left(M\bar{p} - q_0\right)^2 = 2\beta\left(\bar{p} - p_0\right) \tag{26}$$

The parabola also goes through the origin, thus

$$q_0^2 = -2\beta p_0 \tag{27}$$

When the OCR is equal to infinite, the slope of the parabola should be equal to 3. So the following equation can be obtained by differentiating Equation (25)

$$\left(\partial q_f / \partial p\right)\Big|_{(0,0)} = -\beta / q_0 = 3 \tag{28}$$

The values of p_0, q_0 and β can be solved by combing Equations (26)-(28). And finally the expression for the parabola can be obtained

$$q_f = \sqrt{\frac{-3M^2\bar{p}}{M-3}\left(p - \frac{M\bar{q}}{12(M-3)}\right)} + \frac{M\bar{q}}{2(M-3)} \tag{29}$$

As $\bar{p} = p/R$, the following equation can be obtained by letting $k = \dfrac{M^2}{12(3-M)}$

$$q_f = \sqrt{36k\frac{p}{R}\left(p + k\frac{p}{R}\right)} - 6k\frac{p}{R} \tag{30}$$

So the potential failure stress ratio is expressed as

$$M_f = \frac{q_f}{p} = 6\left[\sqrt{\frac{k}{R}\left(1 + \frac{k}{R}\right)} - \frac{k}{R}\right] \tag{31}$$

The responses of UH model with the original and revised Hvorslev envelops are compared in Figure 2. Simulations are conducted under drained constant-p triaxial compression conditions with the model parameters obtained by Yao et al. [32]. For the UH model with the original Hvorslev envelope, when the OCR is 100 or 200, the peak stress ratio is greater than 3. Higher peak stress ratio can be predicted when the OCR is even larger. This is obviously not realistic. The UH model with the modified Hvorslev envelop can reproduce more reasonable results in regard to the peak strength. The predicted peak stress ratio can never exceed 3.

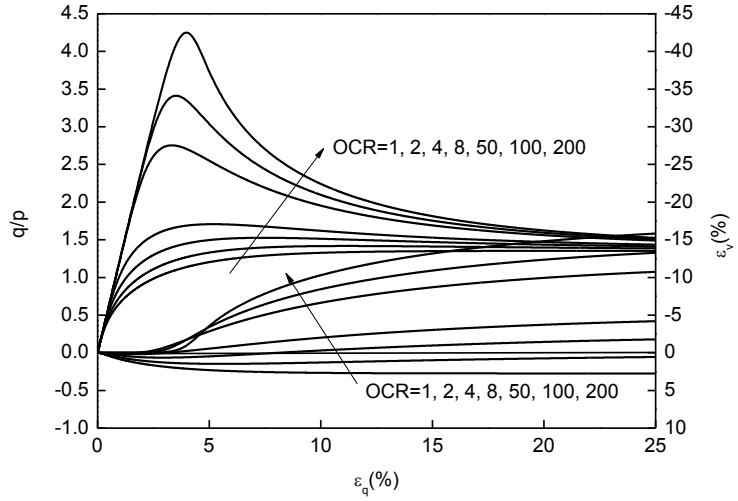

(a)

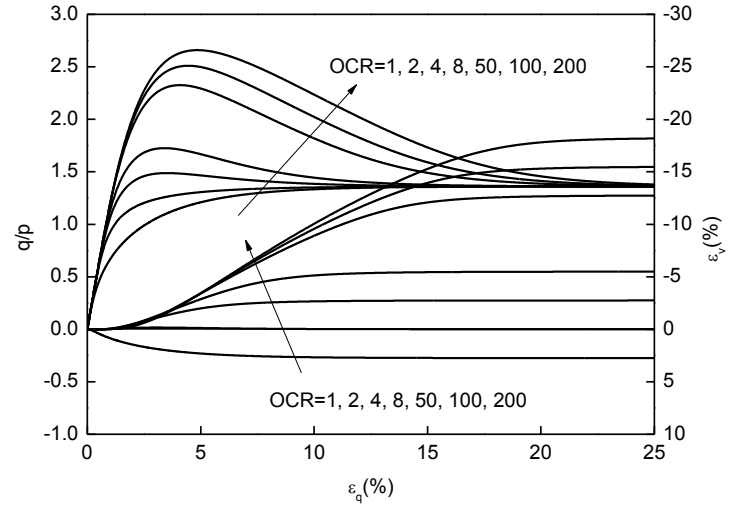

(b)

Fig. 2. Responses of the UH model with (a) the original Hvorslev envelope and (b) the

revised Hvorslev envelop under constant-p compression conditions

The SMP criterion [33, 34] is one of the best in describing both the shear yield and failure behaviors of soils in the three-dimensional stress space, but its irregular geometry in the π-plane makes it difficult to be applied to constitutive models like the modified Cam-Clay model. The transformed stress tensor deduced by Yao et al. can solve this problem satisfactorily [35, 36]. The transformed stress tensor is deduced by making the SMP curve in the π-plane a circle, as displayed by the dotted line of Figure 3 with the center being the origin in the transformed π-plane. The transformed stress tensor has already been applied to the constitutive modeling for both sand and clay, and satisfactory results have been obtained [37-39].

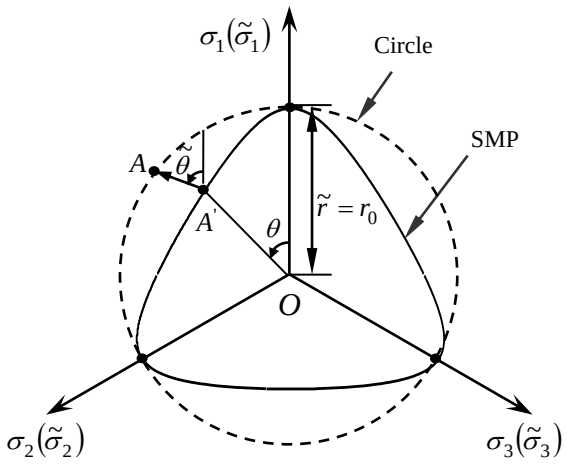

Fig. 3. Transformed relationships based on the SMP criterion

The transformed stress tensor $\tilde{\sigma}_{ij}$ can be written as [32]

$$\tilde{\sigma}_{ij} = p\delta_{ij} + \frac{q^*}{q^s}\left(\sigma_{ij}^s - p^s\delta_{ij}\right) \tag{32}$$

where

$$p^s = \frac{1}{3}\sigma_{ii}^s, \quad q^s = \sqrt{\frac{3}{2}\left(\sigma_{ij}^s - p^s\delta_{ij}\right)\left(\sigma_{ij}^s - p^s\delta_{ij}\right)}, \quad \sigma_{ij}^s = \left(I_1^s\sigma_{ik} + I_3^s\delta_{ik}\right)\left(\sigma_{kj} + I_2^s\delta_{kj}\right)^{-1} \tag{33}$$

$$I_1^s = \sqrt{\sigma_1} + \sqrt{\sigma_2} + \sqrt{\sigma_3}\ , \quad I_2^s = \sqrt{\sigma_1\sigma_2} + \sqrt{\sigma_2\sigma_3} + \sqrt{\sigma_3\sigma_1}\ , \quad I_3^s = \sqrt{\sigma_1\sigma_2\sigma_3} \tag{34}$$

The UH model can be easily generalized to the three-dimensional stress space by using the transformed stress tensors [32].

5. Model Comparisons and Test Verification

In this section, the capabilities of three models are compared and analyzed. The analysis process is carried out according to the three typical models in detail.

5.1. Analysis of Model Principle

(1) BS model

The operating principle of the boundary surface model is that in the p-q space, the boundary surface is composed of two ellipses and a hyperbola, and the overall shape is close to an ellipse. By observing the cyclic tensile and compressive test curves of metal materials, it is found that there is a hidden boundary curve in the stress-strain relation curve of metal, which is extended to the principal stress space, and then there should be a boundary surface in the principal stress space. The material stress cannot cross the boundary surface, but can only be inside or reach the boundary surface. Compared with other models, the mapping method is used to correlate the current stress point with the image point on the boundary surface. Using the projection center, an image point is projected on the boundary surface through the current stress point. The function of the distance between the current stress point and the image point is used to reflect the plastic modulus, as well as the hardness of the soil.

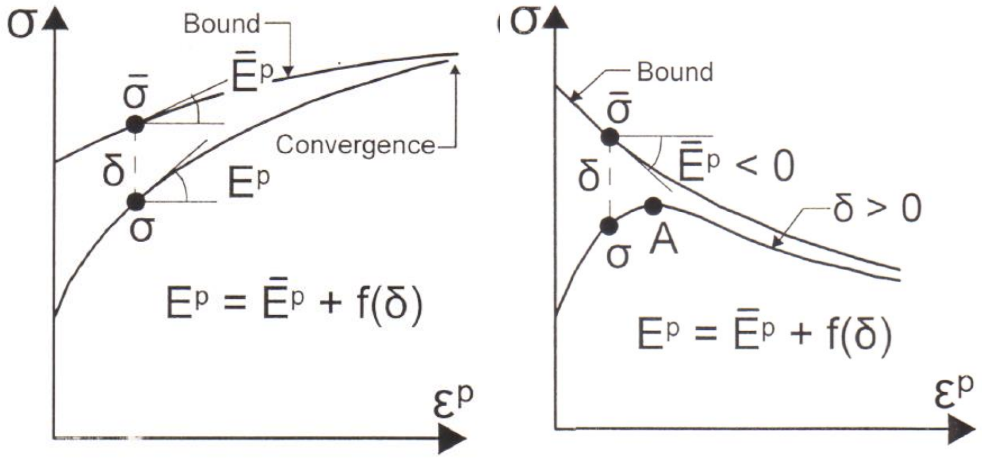

Fig. 4. Typical stress-strain relationship of soils calculated by the BS model (a) stress-strain curve under hardening process; (b) stress-strain curve under softening process

Figure 4 has three main features:

① No matter it's the hardening or softening process, the current stress point is always inside the boundary surface or reaches the boundary surface, and cannot exceed the boundary surface. For soil materials dominated by plastic deformation, when the radius of the elastic domain is zero, the elastic domain degenerates to a point, indicating the current loading point.

② Selection of a reasonable interpolation function of the distance between the current point and the image point can ensure the convergence of the stress-strain curve in the hardening or softening process.

③ The plastic modulus of a material depends on the distance from the current point to the image point where it evolves. When the distance is large, the plastic modulus is large. The smaller is the distance, the smaller is the plastic modulus. When the stress point reaches the boundary surface and coincides with the image point, the plastic modulus degenerates to the one of the boundary surface.

④ The boundary surface acts as an attractor, maintaining a gravitational effect on the current point until it reaches the boundary surface.

(2) SS model

An ellipse is adopted as the yield surface reflecting the normal remolded clay, while a small ellipse with a geometric similarity ratio of *R* is introduced as the loading surface. The current stress point is always on the loading surface. Different from the boundary surface, the subloading surface directly defines the plastic modulus as the interpolation function of the distance between the current point and the boundary surface. While in the SS model, the incremental evolution relation of geometric similarity ratio *R* is given, and the increment of *R* is expressed as the minus function of the incremental plastic strain modulus. The elastoplastic stiffness matrix can be obtained analytically by using the related flow rule. Another feature of the SS model is that there is no elastic domain. When the stress point moves in the normal direction outside the lower loading surface, it is judged as the elastic-plastic loading stage. When it moves normally in the yield plane, it is judged as the elastic unloading stage. Therefore, the SS model can be used to describe the plastic deformation behavior of loading inside the yield surface.

(3) UH model

In the UH model, the yield surface exactly the same as the modified Cambridge model is used as the reference yield surface, while the yield surface with uniform hardening parameters is used as the current yield surface. Similar to the SS model, the current yield surface behaves the same as the lower loading surface. The current stress point is always on the current yield surface. As a state parameter, the similarity ratio *R* between the current yield surface and the reference yield surface is expressed as a parabolic function of the

potential strength M_f in the uniform hardening parameters. Compared with the SS model, the incremental formula of R in the SS model is directly given according to the experimental rules, with subjective factors; while the evolution formula of R in the UH model is a full expression, which is directly expressed by the reference yield surface.

For the above three models, the following differences exist:

① The definitions of elastoplastic behavior are different. All three models are elastic-plastic models. The boundary surface model is still within the framework of classical elastic-plastic theory, and there is always a pure elastic domain. Only when the stress point crosses the elastic domain, it enters the elastoplastic stage. However, the SS model and UH model do not belong to the classical elastic-plastic theory. The loading stage belongs to the elastic-plastic behavior stage, while the unloading stage belongs to the elastic behavior.

② The expressions of elastic-plastic modulus are different. The plastic modulus of BS model is the interpolation function constructed by the distance between the stress point and its image point. And the boundary surface is the yield surface that obeys the related flow law. Therefore, the plastic modulus of the current stress point is an interpolation function reflecting the modulus of the boundary surface. The SS model and UH model are based on the lower loading surface or the current yield surface, subject to the associated flow rule, to calculate the incremental plastic modulus.

③ Regardless of whether the BS model or the SS model simulates the model under true three-dimensional stress condition, it adopts the g(θ) method; that is, it adopts the shape function to modify the coefficient of critical state strength parameters. The UH model

adopts the method of transforming stress, based on the strength criterion of SMP. The difference between the two generalization methods is that taking the g(θ) method is only a numerical correction of the strength parameters in the critical state; while taking the transformation stress method, the yield surface takes the shape of SMP in the offset plane at each increment step. And the main differences are as follows: with the increase of hydrostatic pressure, the stress-induced anisotropy will occur in geotechnical materials under the influence of hydrostatic pressure. In the small spherical stress range, the off-plane shape is close to the sharp curvilinear triangle. In the large spherical stress range, the off-plane shape is close to the circle. However, as the g(θ) method is only adopted to modify the size of the critical state parameter M, the stress-induced anisotropy caused by the above hydrostatic pressure cannot be properly reflected.

④ When the initial axis of symmetry of the yield surface is not the p-axis, but in the line of K_0 consolidation, namely for the initial anisotropy model, then if the g(θ) method is still applied, due to the yield surface axis of symmetry in the principal stress deflection angle of a space, at this point, the g(θ)-method-modified yield surface in the principal stress space will be outside the closed form of convex. The convexity of the yield surface is still guaranteed by the method of transformation stress.

5.2. Parameters for the Models and Their Determination Techniques

In this section, the capabilities of addressing the behavior of OC clays of the BS model, SS model and UH model are analyzed by comparing their predictions with the test results. The tests were carried out by Shimizu [40] on the saturated Fujinomori clay under constant mean effective stress paths to investigate the dilatancy of OC clays. All the

samples were first isotropically consolidated to p_c=588 kPa and then unloaded to achieve different OCRs. The physical properties of the clay are described in [40].

The equivalent mean normal stress p_e is defined as

$$p_e = p_u \exp\left(\frac{N-e}{\lambda}\right) \tag{35}$$

where p_u (=100 kPa) is the reference mean stress, N is the void ratio at the point on the normal consolidation line (NCL) for the reference stress p_u, and e is the current void ratio. The value of N is 0.9108 for the Fujinomori clay [40]. The CSL in the e-p space is

$$e_c = \Gamma - \lambda \ln\left(p / p_u\right) \tag{36}$$

where Γ is the void ratio at the point on the CSL for the reference stress p_u, and e_c is the critical state void ratio at mean stress p. The value of Γ is 0.8448 for the Fujinomori Clay [40].

The common material parameters for the three models are shown in Table 1. The parameters λ, κ, and M are determined from the test data directly. The Poisson's ratio ν is determined empirically as it does not affect the overall responses of these models significantly.

There are totally sixteen parameters for the BS model. The parameters I_l, m, and s can be assumed constant, so their values are the same as those proposed by Dafalias and Herrmann [19]. The parameters R_c, A_c, T, C and h_c are determined from the drained triaxial compression test data using the trial-and-error method. Since the triaxial extension test data on the Fujinomori clay are not available here, the parameters for triaxial extension (R_e, A_e, h_e, and N_e) are not determined. So, only twelve of the model parameters are listed in this paper.

There are five parameters for the SS model. The parameter ϕ is the friction angle of the Fujinomori clay, which can be back calculated from the value of *M*. The parameter *u* is determined by trial-and-error to best fit the test data.

The four parameters for the unified UH model are just the common ones.

5.3. Predictions and Test Results

There are three groups of data, the p/p_e-q/p_e relation, $q/p-\varepsilon_v$ relation and $q/p-\varepsilon_q$ relation, where ε_v and ε_q are the volumetric and deviatoric strains, respectively. The OCRs for these tests are 1, 1.5, 2, 4, 8 and 20. All these relations will be compared with the model predictions in the following section.

The comparisons between the predictions and test data are shown in Figures 5-7. The solid lines are the model predictions and the hollow marks are the test data. The comparisons indicate that all the three models can generally describe the behavior of OC clays. It should be noted that the peak deviatoric stress *q* predicted by the BS model is very

Table 1. Common material parameters for the BS model, SS model and UH model

λ	κ	M	ν
0.1146	0.0247	1.4	0.1

Table 2. Parameters for the BS model

N_c	R_c	A_c	T=C
0.2694	2	0.02	0
h_c	I_l	m	s
6.0	10 kPa	0.02	1

Table 3. Parameters for the SS model

φ	u
33.7°	5

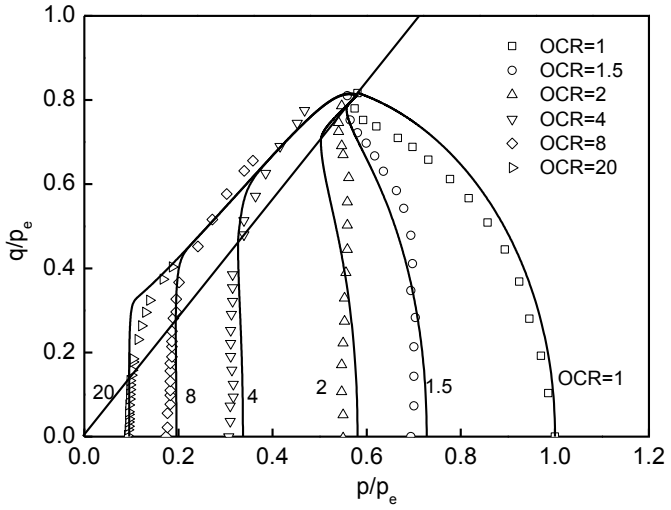

(a)

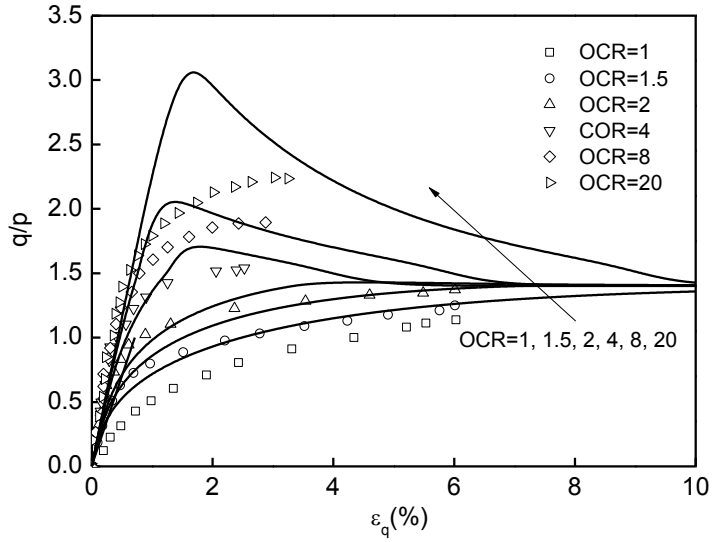

(b)

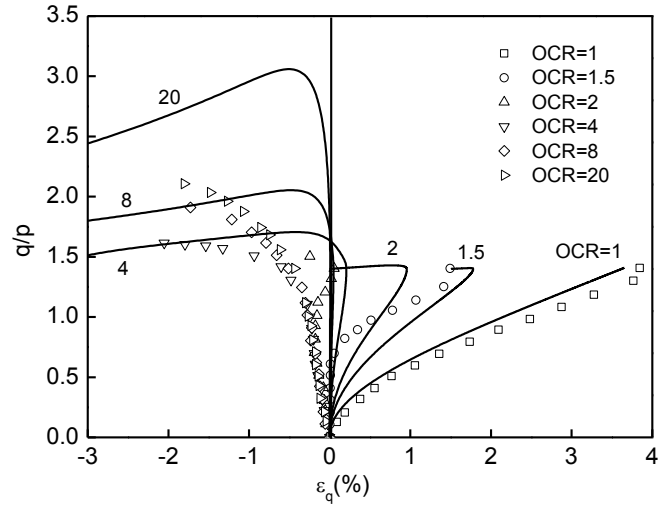

(c)

Fig. 5. Predictions of the BS model and test data: (a) p/p_e-q/p_e relation; (b) $q/p-\varepsilon_v$ relation and (c) $q/p-\varepsilon_q$ relation

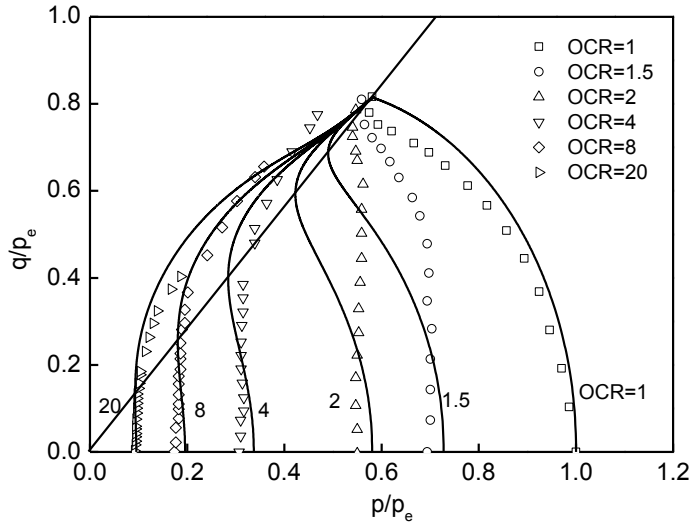

(a)

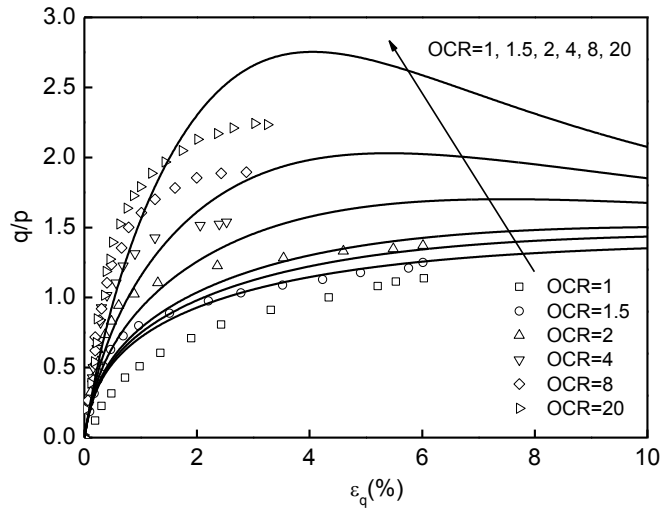

(b)

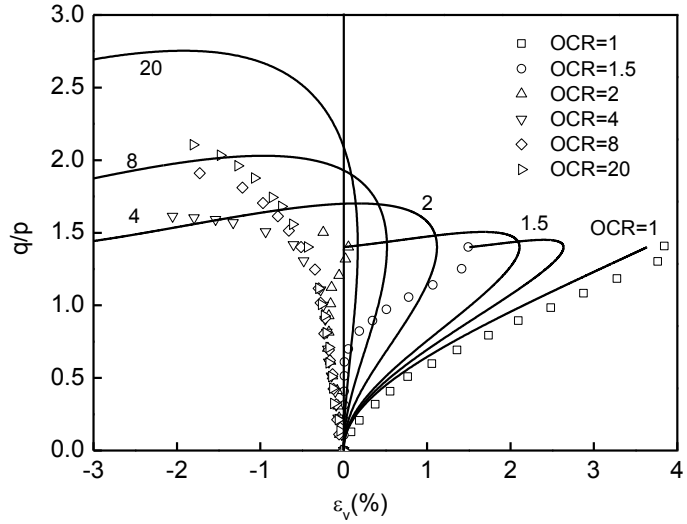

(c)

Fig. 6. Predictions of the SS model and test data: (a) p/p_e-q/p_e relation; (b) $q/p-\varepsilon_v$ relation and (c) $q/p-\varepsilon_q$ relation

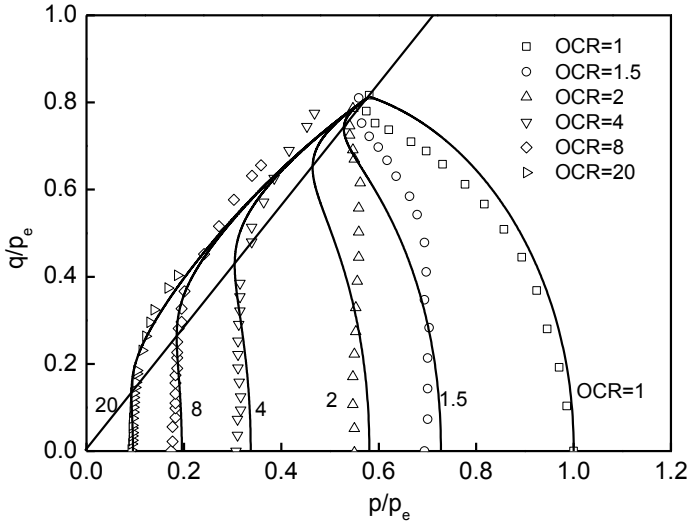

(a)

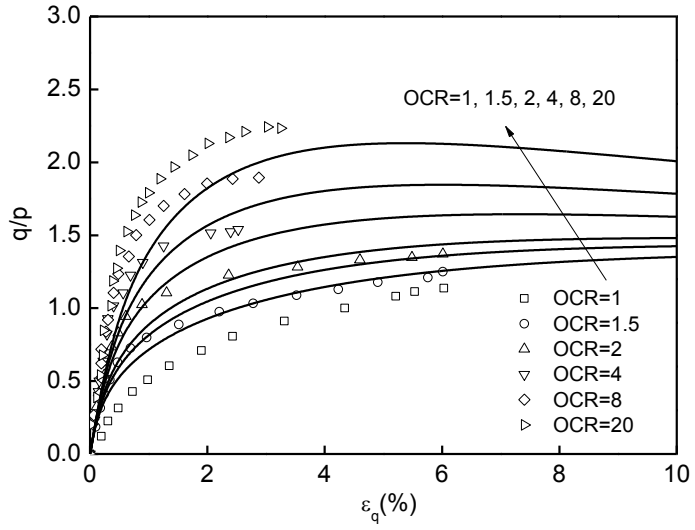

(b)

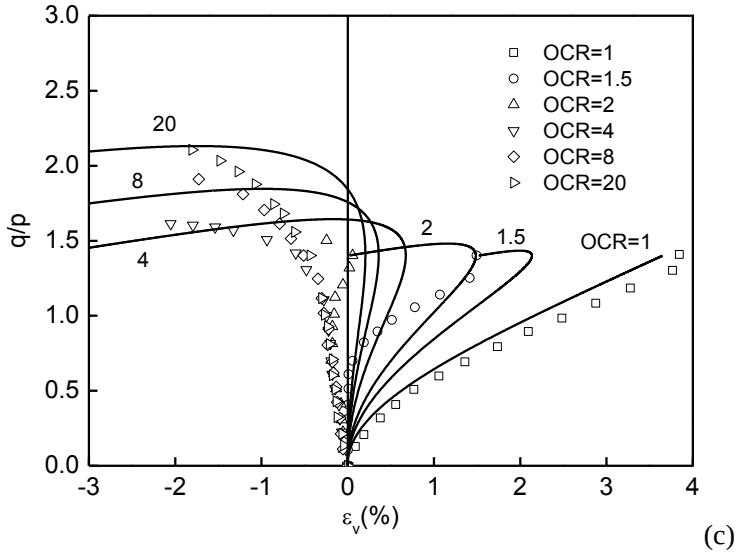

Fig. 7. Predictions of the UH model and test data: (a) p/p_e-q/p_e relation; (b) $q/p-\varepsilon_v$ relation and (c) $q/p-\varepsilon_q$ relation

close to the test data, but the predicted peak strength ratio is higher. The SS model also over-predicts the peak stress ratio. This is due to the shapes of the BS for the BS model and the normal yield surface for the SS model, respectively. The UH model has a better control over both the peak deviatoric stress and peak stress ratio, which is because of the employment of the revised Hvorslev envelop. Figures 8(a)-(c) show the responses of the three models under undrained triaxial compression conditions. The upper parts of the figures show the predicted effective stress paths normalized by the pre-consolidation pressure p_0. The lower parts show the predicted relations between p/p_0 and void ratio e. These figures clearly demonstrate that all the three models can describe the attainment of the critical state of OC clays, at which both the stress and volume remain constant while the plastic deviatoric strain keeps increasing.

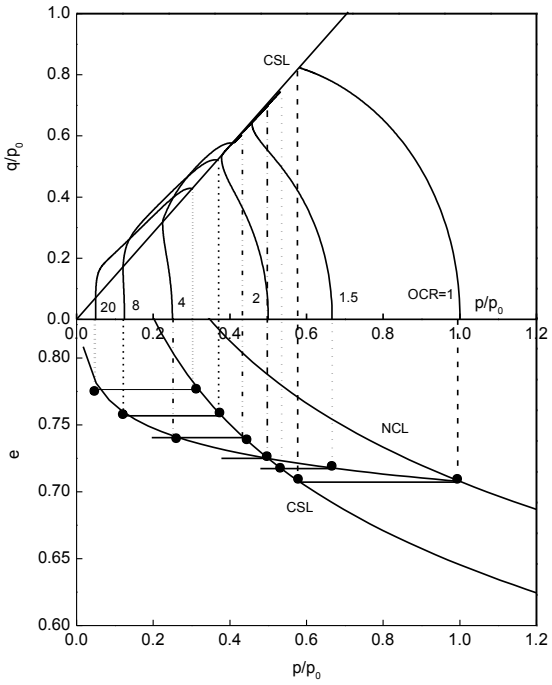
CSL
20
8
4
2
1.5
OCR=1
p/p0
q/p0
NCL
CSL
e
p/p0

(a)

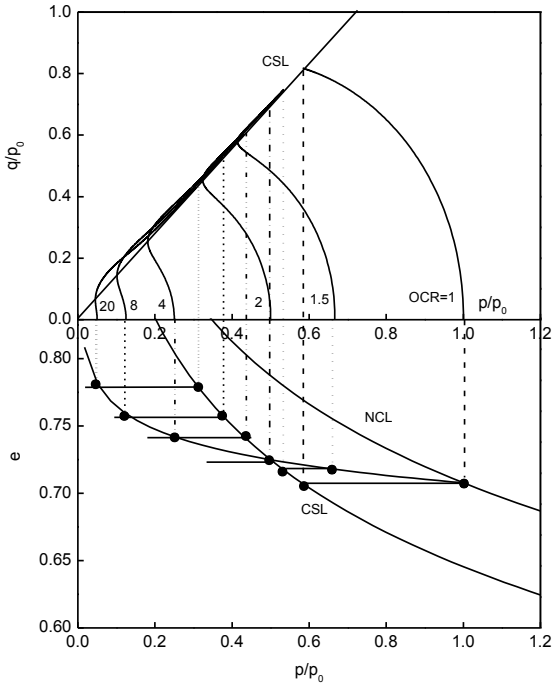
CSL
20
8
4
2
1.5
OCR=1
p/p0
q/p0
NCL
CSL
e
p/p0

(b)

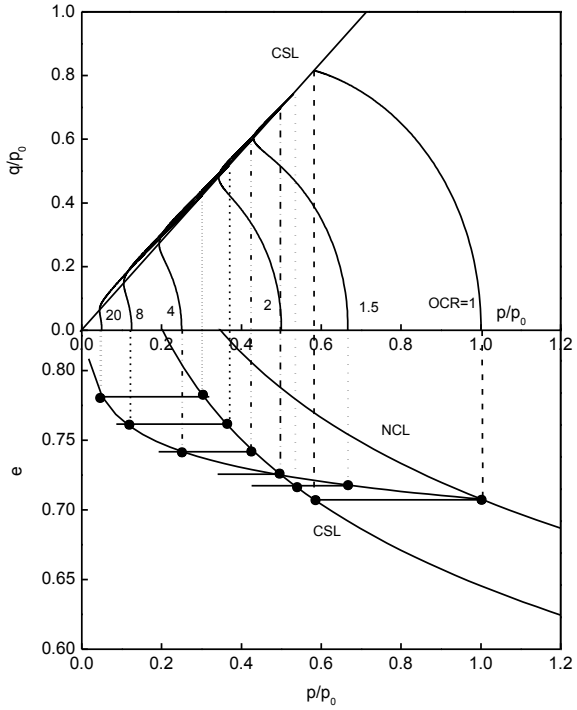

(c)

Fig. 8. Illustration of the responses of the (a) BS model; (b) SS model and (c) UH model under undrained triaxial compression conditions

The employment of the transformed stress tensor based on the SMP criterion is a very important feature of the UH model, which is discussed in detail by Yao et al. [32] Both the strength characteristics and plastic flow directions can be described by the UH model in the three-dimensional stress space through employing the transformed stress tensor. Different $g(\theta)$ methods are adopted to generalize the BS and SS models to the three-dimensional stress space. But using such methods always needs introduction of additional parameters or new interpolation functions. In fact, the transformed stress tensor can also be used to generalize other models like the BS and SS models for isotropic materials into the three-dimensional stress space.

In order to reflect the deformation and strength characteristics of clay under general stress conditions, and to show the influence of intermediate principal stress on strength and

deformation, the test results of three models under the true triaxial stress paths shown in Figure 9 were selected for prediction and comparison. The loading stress paths with the Lode angle being 0°, 15°, 30°, 45°, and 60°, respectively, are shown in Figure 9. The experimental results are the test data of true triaxial stress loading carried out by Chowdhury et al. on saturated Fujinomori clay. The spherical stress remains constant at 196 kPa. The initial void ratio is 0.786, and the parameters used in the model are shown in Tables 4-6.

Table 4. Common material parameters for the BS model, SS model and UH model

λ	κ	M	ν
0.09	0.02	1.38	0.3

Table 5. Parameters for the BS model

N_c	R_c	A_c	T	C
0.2617	2	0.04	0.04	0.02
h_c	I_l	m	s	
79	10 kPa	0.02	1	

Table 6. Parameters for the SS model

φ	u
34°	5

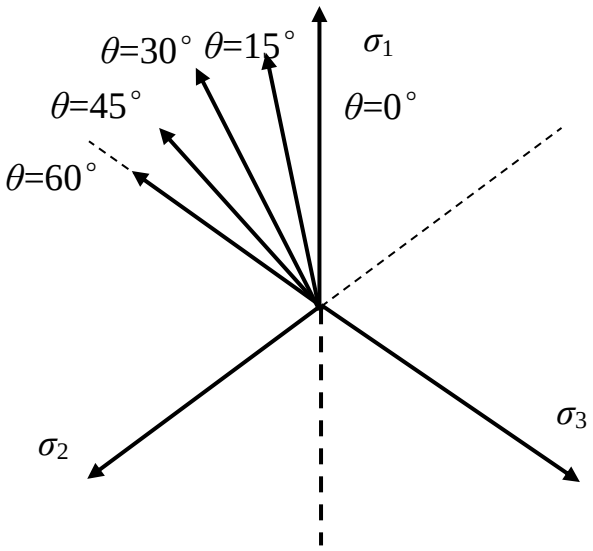

Fig. 9. The true triaxial stress paths on a deviated plane

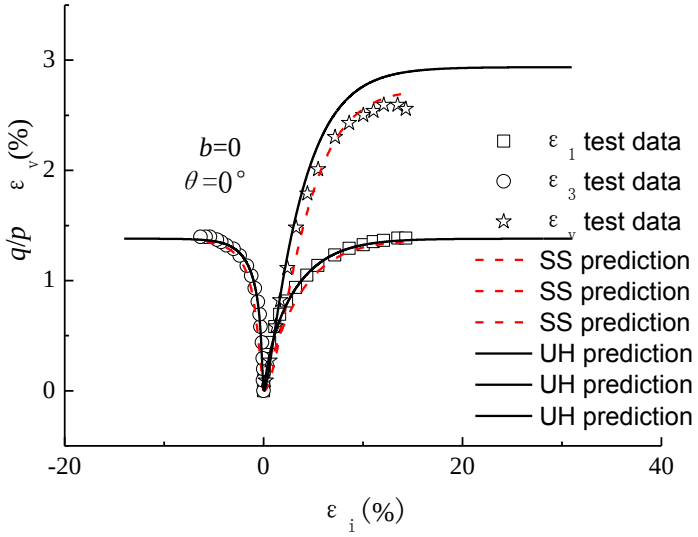

Fig. 10. Comparison of prediction and test results of SS model and UH model under triaxial compression test

In Figure 10, the test results under the constant-p triaxial compression of SS model and UH model are used for predictive comparison. As can be seen from the comparison, for the prediction results of the relationship curve between major principal strain and minor principal strain and stress ratio, the SS model slightly underestimates the stress ratio, while the UH model well predicts the strain and stress ratio curve. For the prediction of volume

strain, the SS model is slightly better than the UH model.

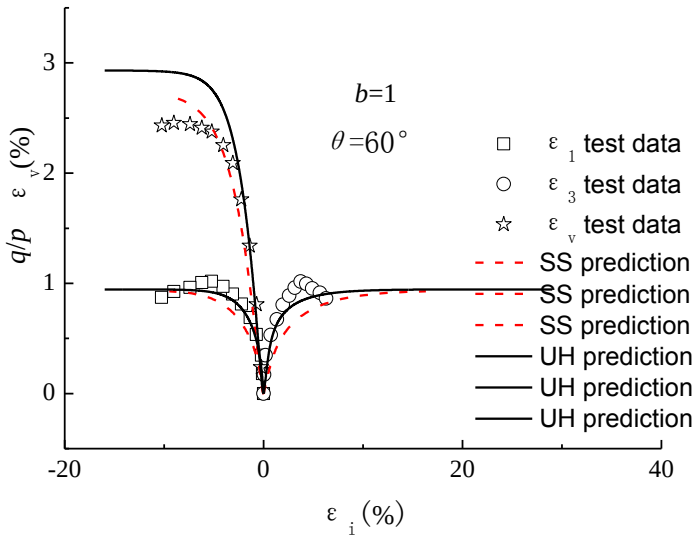

Fig. 11. Comparison of prediction and test results of SS model and UH model under triaxial extension test

Figure 11 shows comparison of the predicted results under triaxial extension. As for the predicted results of major principal strain and minor principal strain to stress ratio, the predicted results of SS model are lower than those of the test results, while the predicted results of UH model well conform to the stress ratio curve, but are still slightly lower than the tested value of peak stress ratio. As for the prediction of volume strain, the results of the SS model and UH model are both larger than those of the test.

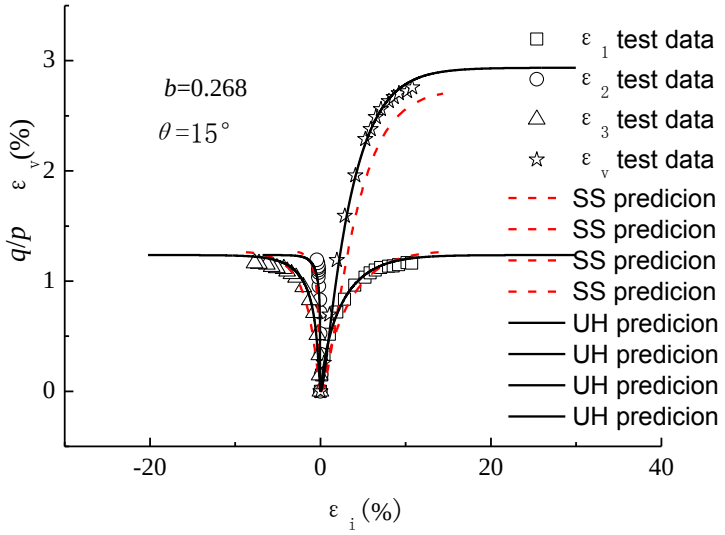

Fig. 12. Comparison of prediction and test results of SS model and UH model under true triaxial test under the SS model with the UH model (θ=15°)

Figure 12 is the prediction comparison results under the condition of Lode angle θ=15°. It can be seen from the comparison results that the SS model still slightly underestimates the stress ratio in the main strain and the stress ratio curves of large and small size. While the UH model well conforms to the stress ratio curve. In the comparison of prediction of volume strain, the predicted results of UH model are basically consistent with the test results, while the predicted results of SS model are slightly smaller.

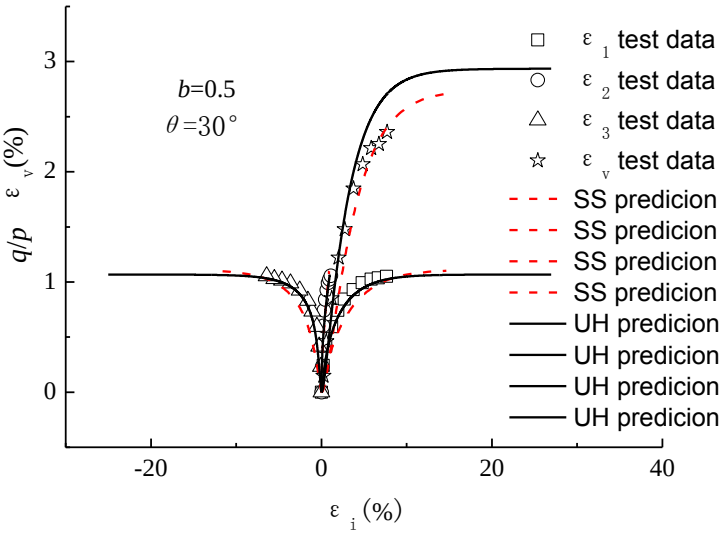

Fig. 13. Comparison of prediction and test results of SS model and UH model under true triaxial test under the SS model with the UH model (θ=30°)

Figure 13 is the prediction comparison results under the condition of Lode angle θ=30°. For strain to stress ratio curves, the UH model still has better prediction results than the SS model. As for the prediction results of the relationship curve of major principal strain and volume strain, both models overestimate the volume strain, but the prediction results of SS model are slightly smaller than those of the UH model.

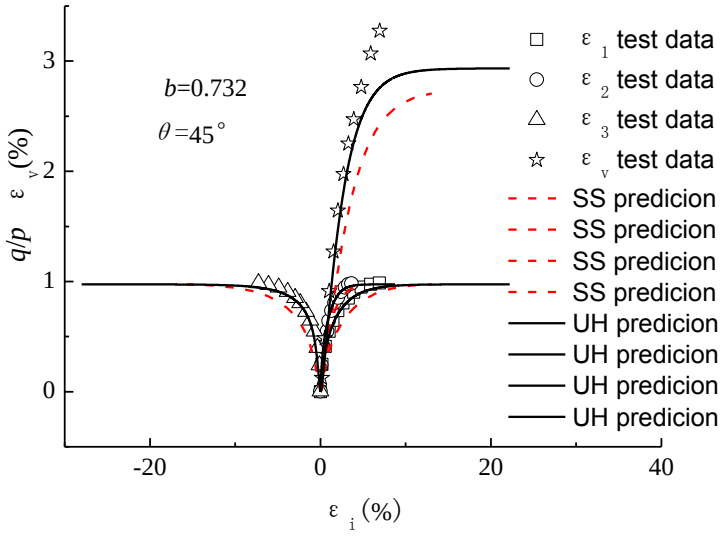

Fig. 14. Comparison of prediction and test results of SS model and UH model under true triaxial test under the SS model with the UH model (θ=45°)

Figure 14 is the prediction comparison results under the condition of Lode angle θ=45°. For the curves of principal strains vs. stress ratio, the UH model results are more consistent with the test results. For the relationship curves of major principal strain and volume strain, both models underestimate the volume strain, but the prediction results of UH model are closer to the test data.

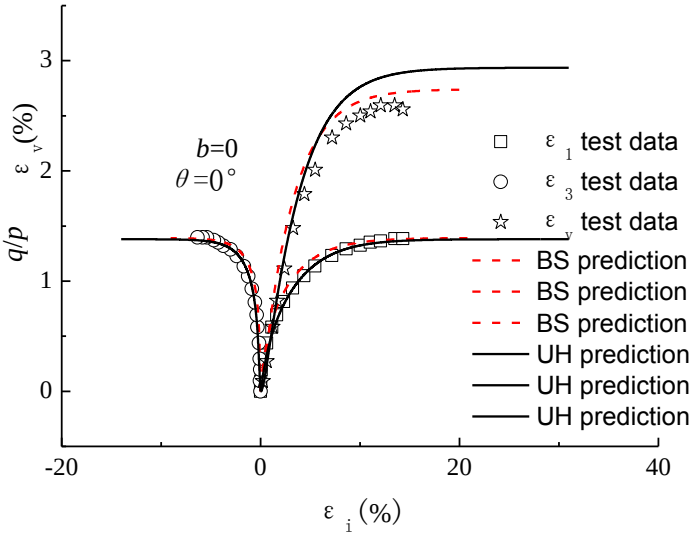

Fig. 15. Comparison of prediction and test results of BS model and UH model under triaxial compression test

Figure 15 shows the comparison of predicted results under triaxial compression. For the curves of principal strains vs. stress ratio, the predicted value of BS model is slightly higher than the result of UH model, and the result of UH model is more consistent with the test result of stress ratio. For the prediction comparison of the relationship curve between major principal strain and volume strain, both models overestimate the volume strain, and the prediction of BS model is closer to the test result of volume strain.

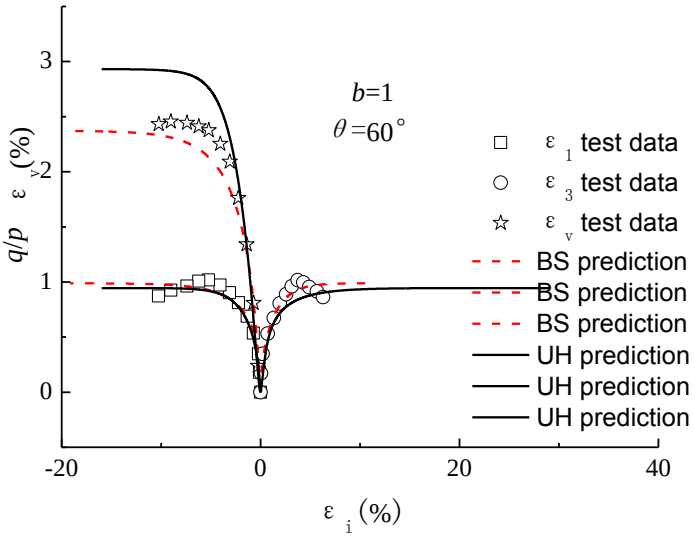

Fig. 16. Comparison of prediction and test results of BS model and UH model under triaxial extension test

Figure 16 shows the test comparison results under the condition of triaxial extension. For the stress ratio curve, the prediction results of BS model are closer to the test data. For the prediction of the relationship between major principal strain and volume strain, the volume strain predicted by the BS model is too low, while the volume strain predicted by the UH model is too high.

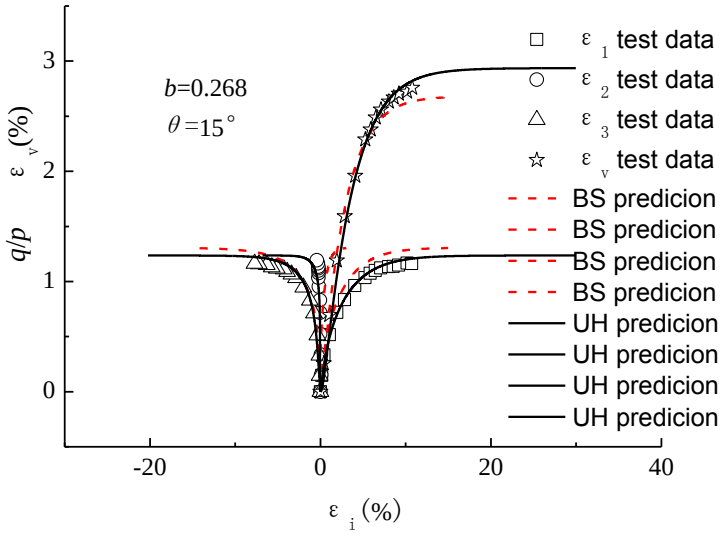

Fig. 17. Comparison of prediction and test results of BS model and UH model under true triaxial test under the SS model with the UH model (θ=15°)

Figure 17 gives the prediction comparison results under the condition of Lode angle θ=15°. The prediction results of UH model accord with the experimental results better. It is particularly noteworthy that, in the prediction of the relationship between the medium principal strain and the stress ratio curve, the medium principal strain is close to zero, but still negative. However, the medium principal strain predicted by the BS model is positive, which is contradictory to the measured results. The prediction results of UH model are negative, which better reproduce the characteristics of medium principal strain.

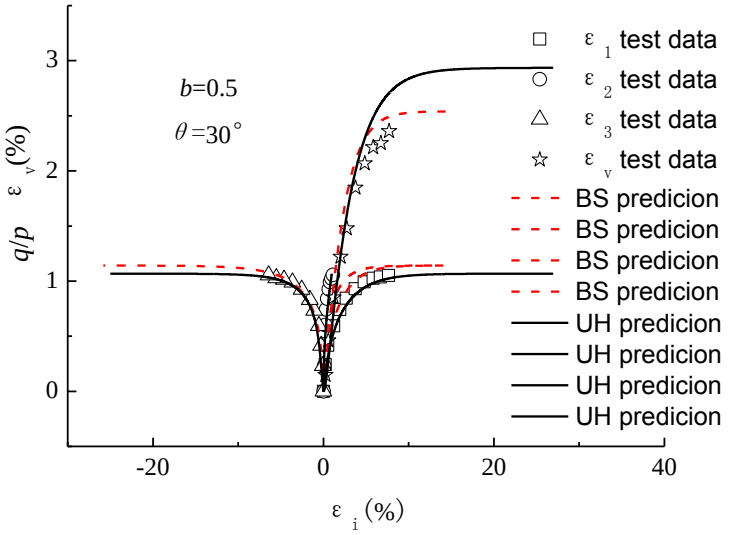

Fig. 18. Comparison of prediction and test results of BS model and UH model under true triaxial test under the SS model with the UH model (θ=30°)

Figure 18 gives the prediction comparison results under the condition of Lode angle θ=30°. The BS model is adopted to compare the relationship curves of strain vs. stress ratio of large, medium and small values. It can be seen that the strength value predicted by BS is slightly higher than the measured value, while the UH model is basically consistent with the measured value. The BS and UH models are used to predict the results of the relationship between major principal strain and volume strain. The prediction results of BS model are closer to the measured values.

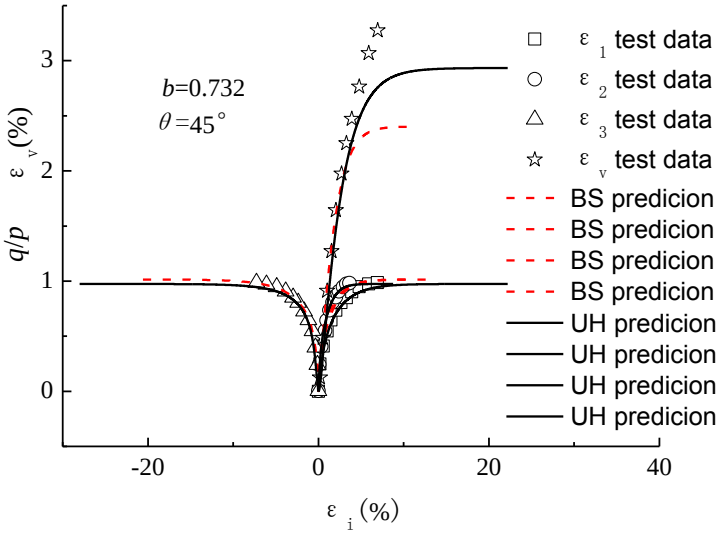

Fig. 19. Comparison of prediction and test results of BS model and UH model under true triaxial test under the SS model with the UH model (θ=45°)

Figure 19 shows the prediction comparison results under the condition of Lode angle θ=45°. As can be seen from the figure, the UH model and BS model are basically consistent with the strength curves of large, medium and small strain and stress ratio. As for the relationship between major principal strain and volume strain, both models underestimate the volume strain, while the prediction of UH model is more consistent with the measured value.

6. Conclusions

In this paper, representative models for OC clays are reviewed. The features of the BS model, SS model and UH model are introduced. Modification is made to the Hvorslev envelop adopted in the UH model to improve its capability of describing the peak strength of highly OC clays. Then the capabilities of describing the behavior for OC clays of three models are analyzed by comparing their predictions for the test data on Fujinomori clay. The following conclusions can be drawn:

(1) These models for OC clays generally fall into two categories, one based on the

classical plasticity theory, and the other the bounding plasticity theory. The classical plasticity theory has its own limitation that no plastic deformation can occur inside the yield surface. The BS plasticity can overcome this deficiency. The BS model, SS model and UH model are representatives for the second type.

(2) The comparison among these three representative models demonstrates that all of them are adequate to describe the main characteristic behaviors of OC clays like strain softening and dilatancy.

(3) The UH model has the fewest parameters with clear physical meanings.

Acknowledgements

This study was supported by the National Natural Science Foundation of China for young scholars (Grant No. 11402260).

REFERENCE

1. Roscoe KH, Schofield AN, Wroth CP. On the yielding of soils. *Géotechnique* 1958; **8**:22–52.
2. Roscoe KH, Schofield AN. Mechanical behaviour of an idealised ‘wet’ clay. *Proceeding of 2nd European Conference on Soil Mechanics and Foundation Engineering*, vol. 1, Wiesbaden, 1963; 47–54.
3. Roscoe KH, Burland JB. On the generalized stress-strain behavior of ‘wet’ clay. *Engineering Plasticity*. Cambridge University Press: Cambridge, 1968; 535-609.
4. Schofield AN, Wroth CP. *Critical state soil mechanics*. McGraw-Hill: London, 1968.
5. Wood DM. *Soil behavior and critical state soil mechanics*. Cambridge University Press: Cambridge, 1990.

6. Pender MJ. A model for the behavior of overconsolidated soil. *Géotechnique* 1978; **28**(1): 1-25

7. Banerjee PK, Stipho AS. Associated and non-associated constitutive relations for undrained behavior of isotropic soft clays. *International Journal for Numerical and Analytical Methods in Geomechanics* 1978; **2**(1): 35-56.

8. Banerjee PK, Stipho AS. An elastoplastic model for undrained behavior of heavily overconsolidated clay. *International Journal for Numerical and Analytical Methods in Geomechanics* 1979; **3**(1): 97-103.

9. Yu HS. CASM: A unified state parameter model for clay and sand. *International Journal for Numerical and Analytical Methods in Geomechanics* 1998; **22:** 621-653.

10. Mroz Z. On the description of anisotropic workhardening. *Journal of the Mechanics and Physics of Solids* 1967; **15**: 163-175.

11. Prévost JH. Mathematical modeling of monotonic and cyclic undrained clay behavior. *International Journal for Numerical and Analytical Methods in Geomechanics* 1977; **1**(2): 195 – 216.

12. Dafalias YF, Popov EP. Plastic internal variables formalism in cyclic plasticity. *Journal of Applied Mechanics,* 1976; **98**: 645-651.

13. Dafalias YF, Popov EP. Cyclic loading for materials with a vanishing elastic region. *Nuclear Engineering and Design*, 1977; **41**(2): 293-302.

14. Hashiguchi K, Ueno M. Elastoplastic constitutive laws of granular materials. *Constitutive Equations of Soils*. Tokyo, 1977; 73-82.

15. Hashiguchi K. Constitutive equations of elastoplastic materials with elasticoplastic

transition. *Journal of Applied Mechanics* 1980; **47**(2): 266-272.

16. Hashiguchi K. Subloading surface model in unconventional plasticity. *International Journal of Solids and Structures* 1989; **25**(8): 917-945.

17. Dafalias YF, Herrmann LR. Bounding surface formulation of soil plasticity. *Soil Mechanics-Transient and Cyclic Loads*. John Wiley and Sons: Chichester, 1982; 252-282.

18. Dafalias YF. Bounding surface plasticity I: mathematical foundation and hypoplasticity. *Journal of Engineering Mechanics* 1986; **112**(9): 966-987.

19. Dafalias YF, and Herrmann LR. Bounding surface plasticity II: application to isotropic cohesive soils. *Journal of Engineering Mechanics* 1986; 1263-1291.

20. Dafalias YF, Herrmann LR. A generalized bounding surface constitutive model for clays. *Application of Plasticity and Generalized Stress-Strain in Geotechnical Engineering*. ASCE: New York, 1982; 78-95.

21. Mroz Z, Norris VA, Zienkiewicz OC. Application of an anisotropic hardening model in the analysis of elastoplastic deformation of soils. *Géotechnique*, 1979; **29**: 1-34.

22. Mroz Z, Zienkiewicz OC. Uniform formulation of constitutive equations for clays and sands. *Mechanics of Engineering Materials.* John Wiley and Sons: Chichester, 1984: 415-449.

23. Whittle AJ, Kavvadas MJ. Formulation of MIT-E3 constitutive model for overconsolidated clays. *Journal of Geotechnical Engineering* 1994; **120**(1): 173-198.

24. Rouainia M, Wood MD. A kinematic hardening constitutive model for natural clays with loss of structure. *Géotechnique* 2000; **50**(2): 153–164.

25. Hashiguchi K, Chen ZP. Elastoplastic constitutive equation of soils with the subloading surface and the rotational hardening. *International Journal for Numerical and Analytical Methods in Geomechanics* 1998; **22**: 197-227.

26. Hashiguchi K, Collins IF. Stress rate-elastic stretching relations in elastoplastic constitutive equations for soils. *Soils and Foundations* 2001; **41**(2): 77-87.

27. Chowdhury EQ, Nakai T, Tawada M. Yamada S. A model for clay using modified stress under various loading conditions with the application of subloading concept. *Soils and Foundations* 1999; **39**(6): 103-116.

28. Nakai T, Hinokio M. A simple elastoplastic model for normally and overconsolidated soils with unified material parameters. *Soils and Foundations* 2004; **44**(2): 53-70.

29. Asaoka A, Nakano M, Noda T. Soil-water coupled behavior of saturated clay near/at critical state. *Soils and Foundations* 1994; **34**(1): 91-106.

30. Asaoka A, Noda, T, Yamada E, Kaneda K, Nakano M. An elasto-plastic description of two distinct volumetric change mechanics of soils. *Soils and Foundations* 2002; **42**(5): 47-57.

31. Noda T. Yamada S, Asaoka A. Elasto-plastic behavior of naturally deposited clay during/after sampling. *Soils and Foundations* 2005; **45**(1):51-64.

32. Yao YP, Hou W, Zhou AN. Three-dimensional unified hardening model for over-consolidated clays. *Géotechnique* 2009; **59**(5):451-469.

33. Matsuoka H. On the significance of the spatial mobilized plane. *Soils and Foundations* 1976; **16**(1): 91-100.

34. Matsuoka H, Nakai T. Stress-deformation and strength characteristics of soil under

three different principal stresses. *Proceeding of the Japan Society of Civil Engineers* 1974; **232**: 59-70.

35. Matsuoka H, Yao YP, Sun DA. The Cam-Clay model revised by the SMP criterion. *Soils and Foundations* 1999; **39**(1): 81-95

36. Yao YP, Zhou AN, Lu DC. Extended transformed stress space for geomaterials and its application. *Journal of Engineering Mechanics* (ASCE) 2007; **133(**10): 1115-1123.

37. Yao YP, Sun DA, Luo T. A critical state model for sands dependent on stress and density. *International Journal for Numerical and Analytical Methods in Geomechanics*. 2004; **28**(4): 323-337.

38. Yao YP, Sun DA, Matsuoka H. A unified constitutive model for both clay and sand with hardening parameter independent on stress path. *Computers and Geotechnics* 2008; **35**(2): 210-222.

39. Yao YP, Yamamoto H, Wang ND. Constitutive model considering sand crushing. *Soils and Foundations* 2008; **48**(4): 603-608.

40. Shimizu M. Effect of overconsolidation on dilatancy of a cohesive soil. *Soils and Foundations* 1982; **22**(4): 121-135.